



ORIGINAL ARTICLE

Fabrication of carboxymethyl functionalized β -cyclodextrin-modified graphene oxide for efficient removal of methylene blue

Ludan Zhao^a, Peixiao Tang^a, Qiaomei Sun^a, Shuangshuang Zhang^a, Zili Suo^a, Huaqing Yang^{a,*}, Xiaoxiang Liao^b, Hui Li^{a,*}

^a School of Chemical Engineering, Sichuan University, Chengdu 610065, Sichuan, PR China

^b Technology Center of China Tobacco Yunnan Industrial Co., Ltd., Yuxi 653100, Yunnan, PR China

Received 18 May 2020; accepted 6 July 2020

Available online 11 July 2020

KEYWORDS

Graphene oxide;
 β -Cyclodextrin;
Carboxymethylated modification;
Adsorption;
Methylene blue

Abstract In this study, a novel carboxymethyl functionalized β -cyclodextrin-modified graphene oxide (CM- β -CD-GO) adsorbent was designed and fabricated. The CM- β -CD-GO was applied to remove methylene blue (MB) from aqueous solutions. The adsorption mechanism was discussed in detail through the study of pH effect, kinetics, and isotherm models. The adsorption of CM- β -CD-GO for MB displayed high removal rates at the pH range of 6.0–10.0, and the removal efficiency is over 90% within 20 min. The pseudo-second-order model could well describe the kinetic process of MB adsorption, and the adsorption was determined by the multi-step process. The maximum uptake capability of CM- β -CD-GO towards MB was 245.70 mg g⁻¹ at 25 °C according to Langmuir isotherm model. A possible adsorption mechanism that electrostatic attraction, π - π interaction, and host-guest supramolecular interactions supported MB adsorption was proposed. The adsorption capacity of CM- β -CD-GO showed no significant change after five cycles. The structure and morphology of CM- β -CD-GO were characterized by XPS, FT-IR, TGA, PXRD, AFM, SEM, zeta (ζ) potential determination, and Raman spectroscopy. This work provides valuable information for the design of novel adsorbents that specifically and efficiently adsorb cationic dyes contaminants.

© 2020 Published by Elsevier B.V. on behalf of King Saud University. This is an open access article under the CC BY-NC-ND license (<http://creativecommons.org/licenses/by-nc-nd/4.0/>).

* Corresponding authors.

E-mail addresses: huaqingyang@scu.edu.cn (H. Yang), lihuilab@sina.com (H. Li).

Peer review under responsibility of King Saud University.



Production and hosting by Elsevier

1. Introduction

Nowadays, a huge amount of wastewater has flowed into the natural water system along with rapid progress of different industries (Geissen et al., 2015; Foroutan et al., 2019). The continuous quality deterioration of natural water resources caused by organic pollutants is a worldwide environmental concern (Alipour and Namazi, 2018; Shabaan et al., 2020). Organic cationic dyes, which are extensively used in papermaking, textile production, leather tanning and other

industries, are harmful to humans and the environment due to their high toxicity and environmental accumulation (Uddin et al., 2009; Yao et al., 2019). Therefore, it is of great significance for environmental protection to remove cationic dyes from contaminated water quickly and effectively.

Dyes can be removed from water systems through various methods, such as adsorption, photocatalysis, chemical degradation and coagulation methods (Karimifard and Moghaddam, 2018; Cerrón-Calle et al., 2019; Zhang et al., 2019). Among these methods, adsorption is the most efficient approach in virtue of its easy operation, low operation cost, and efficiency in dealing with various pollutants (Ali, 2012; Mahmoodi et al., 2013; P. Tang et al., 2019; Y. Tang et al., 2019). Thus, it is necessary to prepare novel facile and efficient adsorbents for the efficient removal of cationic dyes.

Recently, graphene oxide (GO) has been widely investigated and used to remove various contaminants (Rathore and Biswas, 2018; Soleimani et al., 2018; Khadivi et al., 2019). The numerous oxygen-containing functional groups such as carboxyl, hydroxyl and epoxy groups of GO can act as active sites for pollutant adsorption. In addition, abundant π -conjugated aromatic fields exist in the basal plane of GO, and π - π attractions can promote the interaction between GO and compounds containing aromatic nucleus (Chen et al., 2015; Mogha et al., 2020). However, the good dispersibility in aqueous solutions makes it difficult to separate GO, thus limiting its practical usage in pollution management. The modification of GO has been developed as a promising method to address this defect (Kuila et al., 2012). There have been some research reports on the application of GO modified with PEI (Zhu et al., 2013) and octadecylamine (Mingqian et al., 2018) in the adsorption of dye pollutants. β -Cyclodextrin (β -CD) is an environmentally friendly cyclic oligosaccharide composed of several pyranose units linked by glycosidic bond. The nonpolar cavity of β -CD can selectively combine with organic pollutants to form a stable host-guest inclusion complex. Moreover, the β -CD cavity features a high concentration of hydroxyl group internally and externally and high activity, which enable its grafting to various materials. β -CD has been widely used in pollutant treatment because of its unique structural properties (Badruddoza et al., 2017; P. Tang et al., 2019; Y. Tang et al., 2019). To date, many studies have been conducted on β -CD-modified GO (Liu et al., 2014; Einafshar et al., 2018). However, studies have rarely reported the further functionalization of GO grafted with β -CD to adsorb specific dye pollutants.

Considering the unique properties of GO and β -CD, a novel material that simultaneously possesses two unique properties can be obtained by modifying GO with β -CD. Notably, both β -CD and GO contain many oxygen-containing functional groups, which allow the new material to be further functionalized with carboxyl groups. Thus, we propose to prepare anionic adsorption material based on GO and β -CD to improve the removal efficiency of cationic dye pollutants. In this study, carboxymethylated β -CD-modified GO (CM- β -CD-GO) adsorbent, an easily separable material, was fabricated in two steps. We expect the resulting electronegative adsorption material CM- β -CD-GO features excellent removal capability for the model cationic dye methylene blue (MB) because of the carboxymethylation. This study aimed at investigating the adsorption behavior and mechanism involved in the removal of MB by CM- β -CD-GO. The performance of CM- β -CD-GO were evaluated by studying the effects of pH value on the removal efficiency, adsorption kinetics, adsorbent isotherms, and regeneration capability. The possible adsorption mechanism was further analyzed by performing X-ray photoelectron spectroscopy (XPS). This work provides valuable information for the efficient removal of cationic dye contaminants from aqueous solutions.

2. Experimental section

2.1. Materials

Commercially available GO was purchased from Hengqiu Tech. Inc (Jiangsu, China). β -CD (purity > 99%) was

obtained from Chron Chemicals (Chengdu, China). Hexamethylene diisocyanate (HDI) was obtained from Aladdin (Shanghai, China). Chloroacetic acid and MB trihydrate (purity > 99%) were purchased from Huaxia Reagent Co., Ltd (Chengdu, China).

2.2. Preparation of CM- β -CD-GO

The preparation of CM- β -CD-GO included two main steps. First, the GO powder was ultrasonically dispersed in 50 mL DMF (10 mg ml⁻¹) for 1 h. Then 1.78 g HDI (10 mM) and 2 drops of the catalyst Tin 2-ethylhexanoate were added. The suspension was refluxed in nitrogen atmosphere for 3 h at 80 °C. After dissolving 9.08 g β -CD (8 mM) in 50 mL DMF and adding two drops of Tin 2-ethylhexanoate, β -CD solution was added dropwise to the GO suspension. The mixture was further refluxed in nitrogen atmosphere for 3.5 h at 70 °C. The reaction product (β -CD-GO) was obtained by filtration and washing with DMF, and then drying in vacuum at 60 °C for 12 h.

Secondly, the obtained β -CD-GO powder was further subjected to carboxyl functionalization. 0.5 g β -CD-GO powder was dispersed in 50 mL DMF, and then added with 0.5 g NaOH and 0.167 g chloroacetic acid. The mixture was stirred at 50 °C for 12 h. Finally, the filtered solid was rinsed several times with DMF, ultrapure water, and ethanol, and then dried in a laboratory vacuum at 60 °C for 12 h.

2.3. Adsorption experiments

The batch adsorption of MB on adsorbent (β -CD-GO and CM- β -CD-GO) were realized by a conical flask equipped with magnetic stirrers (25 °C, agitation speed 500 r/min). Under magnetic stirring, target adsorbent was dispersed into the dye solution (20–200 mg L⁻¹ for MB) for a certain time. HCl and NaOH solutions were used to adjust the solution pH to 2.0–10.0. At MB concentrations of 100 mg L⁻¹, adsorption kinetics was studied at 25 °C, 35 °C and 45 °C. At a certain designed time, the adsorbents were filtered with a 0.45 μ m inorganic membrane filter, whereas remnant dye was quantified via an ultraviolet detector (UV-1800, Japan) at the maximum absorbance (λ_{max} : 665 nm for MB). Three parallel experiments were carried out in all the tests. The removal efficiency of dyes and adsorption capacity (q_t , mg/g) of adsorbent can be evaluated using Eqs. (1) and (2), respectively:

$$\text{Removal efficiency} = \frac{C_0 - C_t}{C_0} \times 100\% \quad (1)$$

$$q_t = \frac{(C_0 - C_t)V}{m} \quad (2)$$

where C_0 and C_t are the initial and residual concentrations (mg L⁻¹) of the pollutants in the stock solution and filtrate, respectively. V (L) is the solution volume, and m (g) is the adsorbent weight.

2.4. Desorption and reusability

For desorption and reusable study, CM- β -CD-GO was first saturated with a MB solution (100 mg L⁻¹) for 3 h under magnetic stirring. The adsorbent dosage was 0.5 mg mL⁻¹. After

saturation, the solid was separated by filtration, and the MB in the filtrate was quantified by a UV detector. The adsorbents were regenerated by immersion in ethanol at 500 r/min for 1 h, and then rinsed with ultrapure water. The adsorbents were recovered after vacuum drying at 60 °C. The same adsorbent was repeatedly adsorbed/desorbed cycle five times.

2.5. Characterization

The structure and morphology of CM- β -CD-GO were characterized by XPS, Fourier transform infrared spectroscopy (FT-IR), thermal gravimetric analysis (TGA), Raman spectroscopy, powder X-ray diffraction (PXRD) patterns, atomic force microscopy (AFM) and scanning electron microscopy (SEM). The instrument model and measure conditions were provided in [Supplementary Information \(SI\)](#). The zeta (ζ) potential was measured by a NanoBrook Omni analyzer (Brookhaven, USA).

3. Results and discussion

3.1. Remarkable removal of MB by CM- β -CD-GO

The removal of MB, a common cationic dye, by β -CD-modified GO has been studied. However, previous studies involved low removal efficiency and required long equilibrium time ([Liu et al., 2014](#); [Rathour et al., 2019](#)). Given the cationic nature of MB, we hypothesized that the preparation of an anionic material can improve the removal efficiency of MB.

In this study, chloroacetic acid was used for carboxymethyl functionalization to prepare a novel material for improving the MB removal efficiency. [Scheme 1](#) illustrates the synthesis procedure of CM- β -CD-GO. First, the $-\text{N}=\text{C}=\text{O}$ groups of HDI reacted with the oxygen-containing functional group of GO and the hydroxyl group of β -CD to covalently graft β -CD onto GO to prepare β -CD-GO. Second, the carboxymethyl functionalization of β -CD-GO with chloroacetic acid occurred. The electronegative adsorption material CM- β -CD-GO was prepared. Since it was rich in carboxyl groups, we predicted that CM- β -CD-GO features excellent removal capability for MB.

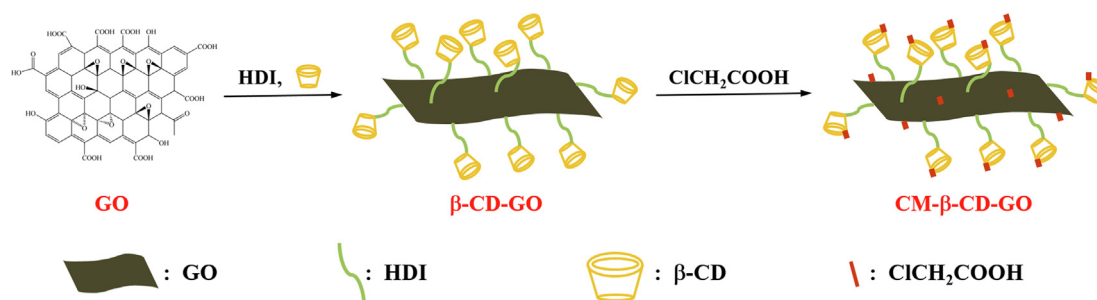
The removal performance of β -CD-GO and CM- β -CD-GO toward MB were examined at a pH of 7 and a temperature of 25 °C. As shown in [Fig. 1a](#), the removal efficiency of CM- β -CD-GO was significantly higher than that of β -CD-GO. Approximately 89.3% of MB was adsorbed on CM- β -CD-GO at 15 min and reached equilibrium after 20 min. The

removal rate was 93.8%, and the equilibrium adsorption capacity reached 187.60 mg g⁻¹. Meanwhile, β -CD-GO adsorbed 22.1% MB under the same conditions. Under similar pH and temperature conditions, the equilibrium adsorption capacity of CM- β -CD-GO obtained in this work was higher than that of graphene oxide material modified by β -CD previously reported; furthermore, the adsorption equilibrium time was significantly faster than those of the materials ([Liu et al., 2014](#); [Rathour et al., 2019](#)). These results indicated that β -CD-GO carboxymethylation increased the number of adsorption sites, and the CM- β -CD-GO displayed more ultrafast adsorption properties than β -CD-GO. In view of the significant removal performance of CM- β -CD-GO on MB, we further explored its adsorption mechanism by determining the influence of pH value of solution on the removal efficiency, kinetics for adsorption processes, adsorption isotherms, and recycling.

3.2. Effect of pH on adsorption

Solution pH is considered as an important factor in cationic dyes adsorption. Thus, we examined the effect of pH on adsorption. It can be seen from [Fig. 1b](#), MB uptake by β -CD-GO was slightly influenced by pH and exhibited poor adsorption capacity. Nevertheless, the influence of pH became significant when β -CD-GO was carboxymethylated. The sorption capacity of CM- β -CD-GO for MB increased considerably with pH, and then reached equilibrium at pH 6.0 (removal efficiency 98%). Thus, the solution pH was not adjusted in the adsorption experiment. These phenomena might be associated with the presence of numerous carboxyl groups on CM- β -CD-GO. With the increase of pH, the carboxyl groups were deprotonated and showed strong negative electricity. Thus, they could interact with additional cationic MB and achieve a high removal efficiency.

To further explain the effect of pH value of solution on the removal efficiency, we measured the zeta potentials at different pH ([Fig. 1c](#)). The β -CD-GO exhibited a positive charge in the pH range of 2.0–7.0 because its hydroxyl groups were protonated. Furthermore, the existence of electrostatic repulsion might hinder the adsorption of β -CD-GO to MB. At pH > 7, β -CD-GO was negatively charged, and its adsorption capacity was slightly enhanced with a maximum of 53%. However, CM- β -CD-GO demonstrated a more negative surface zeta potential compared with β -CD-GO. The zeta potential of CM- β -CD-GO was negative at the pH range of 3.0–10.0, gradually enhanced with the increase of pH, and finally



Scheme 1 Illustration for the synthesis procedure of CM- β -CD-GO.

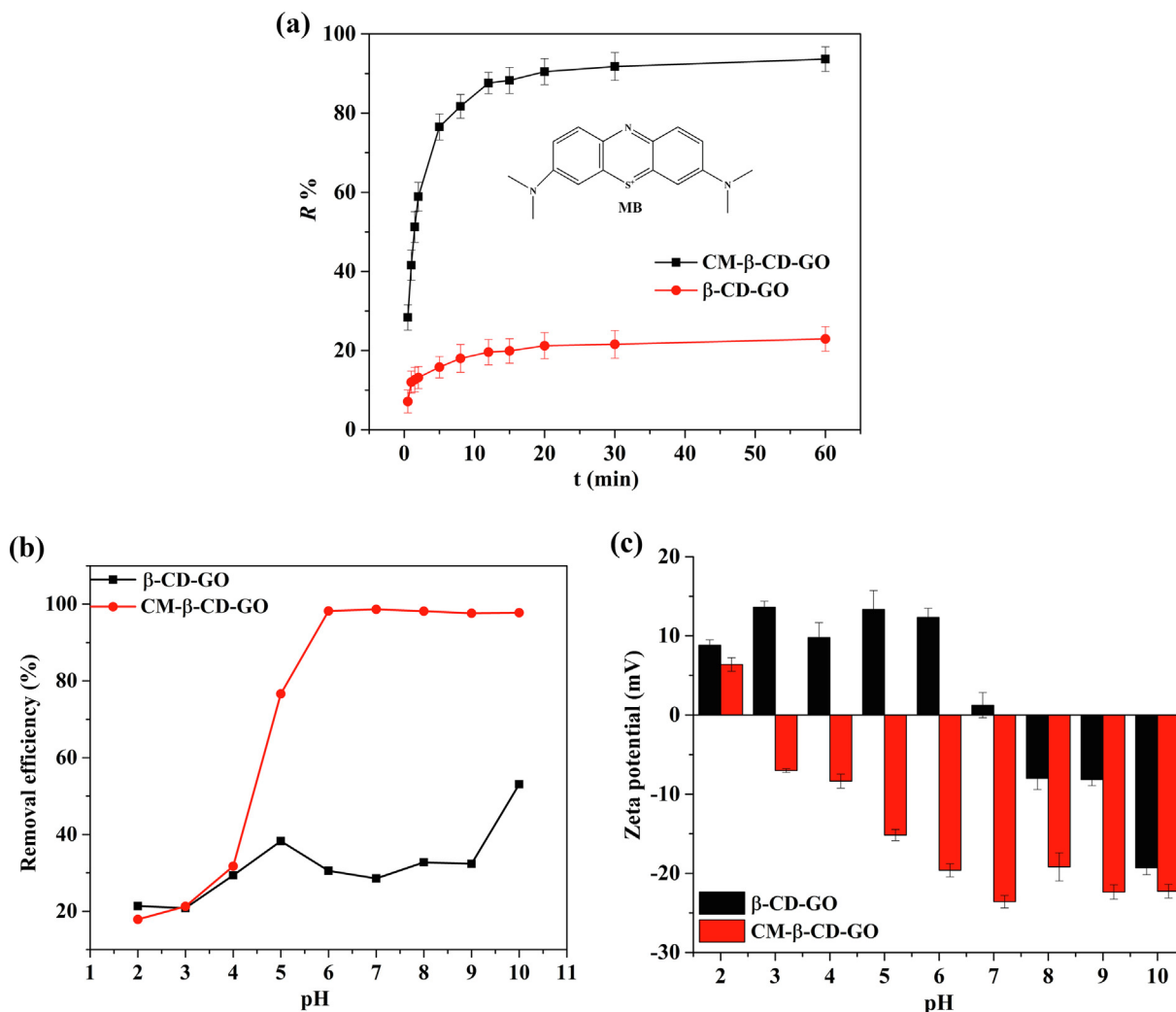


Fig. 1 (a) Removal rate of MB from an aqueous solution on β -CD-GO and CM- β -CD-GO (100 mg L^{-1} MB, 0.5 mg mL^{-1} adsorbent dose, $T = 25 \text{ }^\circ\text{C}$, $\text{pH} = 7.0$), (b) Effect of pH on removal rate of MB (100 mg L^{-1} MB, 0.5 mg mL^{-1} adsorbent dose, $T = 25 \text{ }^\circ\text{C}$, $t = 3 \text{ h}$), (c) zeta-potential curve of β -CD-GO and CM- β -CD-GO in the solution.

remained relatively stable ($-21.40 \pm 2.22 \text{ mV}$) between pH 6–10. The strongest negative charge ($-23.58 \pm 0.79 \text{ mV}$) was observed at pH 7. In terms of electrostaticity, the anionic CM- β -CD-GO is better than β -CD-GO in adsorption of cationic adsorbate MB. These results further indicated that electrostatic forces play a crucial role in the efficient adsorption, and CM- β -CD-GO is suitable for a wide pH range.

3.3. Adsorption kinetics

To fully elucidate the physical chemistry process, we systematically studied adsorption kinetics. Pseudo-first-order and pseudo-second-order models were applied to explore the adsorption mechanism by estimating the removal rate and kinetic parameters (Kausar et al., 2016). The expressions of pseudo-first-order (Eq. (3)) and pseudo-second-order (Eq. (4)) models in nonlinear forms used in this study were as follows:

$$q_t = q_e[1 - \exp(-k_1 t)] \quad (3)$$

$$q_t = \frac{q_e^2 k_2 t}{1 + q_e k_2 t} \quad (4)$$

where q_e and q_t are the uptake capacity (mg g^{-1}) at equilibrium and at time t , respectively; k_1 (min^{-1}) is the pseudo-first-order rate constant; k_2 ($\text{g} [\text{mg}\cdot\text{min}]^{-1}$) is the pseudo-second-order rate constant.

Figs. 2a and S1 shows the nonlinear and linear plots of kinetics models, respectively. The kinetic constants were summarized in Table 1. As presented in Fig. 2a, the adsorption capacity of CM- β -CD-GO occurred rapidly and reached equilibrium at 20 min, which can be attributed to the abundant carboxyl functional groups on CM- β -CD-GO. Furthermore, this phenomenon indicated the minimal mass transfer resistance in the adsorption process and the strong affinity of CM- β -CD-GO for MB dye (Liu et al., 2014). As shown in Table 1, the equilibrium adsorption ($q_{e, \text{cal}}$) of the pseudo-first-order model was inconsistent with the experimental data, and the R^2 values were relatively low. By contrast, the equilibrium adsorption ($q_{e, \text{cal}}$) calculated by the pseudo-second-order model were consistent with the measured values with $R^2 > 0.998$. These result

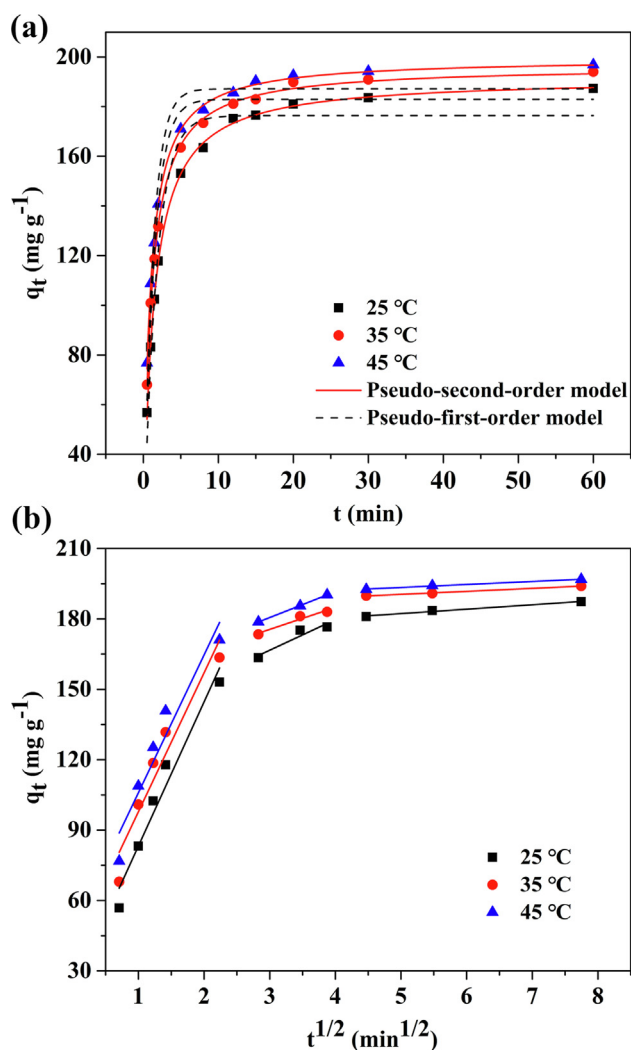


Fig. 2 (a) Adsorption kinetics plots fitted with pseudo-first-order and pseudo second-order model and (b) intraparticle diffusion model for the adsorption of MB onto CM- β -CD-GO (100 mg L⁻¹ MB, 0.5 mg mL⁻¹ adsorbent dose, pH = 7.0).

indicated that the adsorption process accorded with the pseudo-second-order model. These findings implied that the removal of MB by CM- β -CD-GO was related to chemisorption, suggesting that electronic sharing and transfer might exist between the adsorbent and MB.

To further investigate the rate-controlling steps in adsorption process, the intraparticle diffusion model was used to analyze the kinetic results. The intraparticle diffusion model proposed by Weber can be expressed as follows (Weber and Morris, 1963):

$$q_t = k_{di}t^{1/2} + C_i \quad (5)$$

where k_{di} (mg g⁻¹ min^{-0.5}) is the rate constant at stage i , and intercept C_i is proportional to the thickness of boundary layer. Fig. 2b presents the plot of q_t versus $t^{1/2}$ for intraparticle transport. Table 2 presents the values of k_{di} and C_i .

As shown in Fig. 2b and Table 2, the $q_t-t^{1/2}$ plot presents three stages, indicating the high complexity of the adsorption process. The $q_t-t^{1/2}$ plot of the adsorption of MB by CM- β -CD-GO in aqueous phase includes a large intercept and does not pass through the origin. These phenomena mean that another rate-control step existed besides intraparticle diffusion (Chen et al., 2003; Cheung et al., 2007). The first sharp portion represented film diffusion. At this stage, MB diffused rapidly from the bulk solution to the surface of CM- β -CD-GO and then interacted with the active sites and was adsorbed. The second linear portion indicates a gradual adsorption process. The intraparticle diffusion occurred with the MB transferred from the surface of CM- β -CD-GO to the functional group in the pores and intraparticle spaces of adsorbent. At the third stage, the slope of the fitting curve was approach to zero due to the reduced availability of active sites, which indicated that the adsorption process reached equilibrium. As the adsorption reaction proceeded, the boundary layer thickness increased. When ionic interacted to form a thick adsorption layer, the adsorption sites on CM- β -CD-GO were nearly saturated, and the adsorption rate would depend on the intraparticle diffusion of MB. The larger C value indicates the relatively high boundary layer thickness, that is, mass transfer resistance is larger.

In consideration of the kinetics results, the efficient removal process of MB by CM- β -CD-GO was concordant with the pseudo-second-order model. The process included film diffusion, intraparticle diffusion, and equilibrium stages. The adsorption rate of the overall process was multi-step dependent.

3.4. Adsorption isotherms

The distribution of adsorbate molecules in the adsorption process can be described by equilibrium adsorption isotherms, which is very important for the investigation of adsorption mechanism. Langmuir and Freundlich models are commonly employed isotherms. The nonlinear Langmuir (Eq. [6]) and Freundlich (Eq. [7]) models are presented as follows:

$$q_e = \frac{K_L q_m C_e}{1 + K_L C_e} \quad (6)$$

$$q_e = K_F C_e^{1/n} \quad (7)$$

where q_e (mg g⁻¹) is the amount of dyes adsorbed onto the adsorbent at equilibrium; C_e (mg L⁻¹) is the equilibrium

Table 1 Comparison of pseudo first and second order kinetics model constants.

	$q_{e,exp}$ (mg/g)	Pseudo-first-order kinetic model			Pseudo-second-order kinetic model		
		$q_{e,cal}$ (mg/g)	k_1 (min ⁻¹)	R ²	$q_{e,cal}$ (mg/g)	k_2 (g/mg min)	R ²
25 °C	187.63	176.37	0.5852	0.9631	191.64	0.0041	0.9990
35 °C	194.48	182.96	0.7256	0.9512	196.34	0.0053	0.9989
45 °C	196.88	187.15	0.8033	0.9486	199.48	0.0060	0.9987

Table 2 Intraparticle model parameters for the adsorption of MB on CM- β -CD-GO.

	Stage 1			Stage 2			Stage 3		
	k_{d1}	C_1	R^2	k_{d2}	C_2	R^2	k_{d3}	C_3	R^2
25 °C	61.41	21.82	0.9437	13.06	127.49	0.8170	1.88	172.86	0.9737
35 °C	59.19	38.64	0.9033	9.39	147.36	0.9072	1.28	184.07	0.9912
45 °C	58.72	47.22	0.9043	11.03	147.51	0.9996	1.28	187.00	0.9888

concentration of adsorbate; q_m (mg g^{-1}) is the theoretical maximum adsorption capacity; K_L (L mg^{-1}) is a Langmuir adsorption constant; K_F is the Freundlich isotherm constant, and n is the heterogeneity factor related to adsorption intensity.

Fig. S2 shows the nonlinear fitting curves of Langmuir and Freundlich adsorption isotherms of MB, and the specific fitting constants are summarized in Table 3. The R^2 value of the Langmuir model was higher than 0.97. That is, the adsorption process of CM- β -CD-GO to MB could be described by Langmuir model than Freundlich model. This result also implies that MB adsorption was monolayer adsorption, and that once a site was occupied by a dye, it could not absorb other molecules. The maximum q_m value was calculated as 245.70 mg g^{-1} at 25 °C from the Langmuir model. Although the adsorption capacity of CM- β -CD-GO was weaker than that of blank GO, but it was high in the modified GO materials (Table S1). In addition, the value of R_L that provided in SI varied between 0 and 1 (Table S2), signifying the favorability of the adsorption process. This result proves that CM- β -CD-GO was a favorable candidate for the MB removal. The $1/n$ value obtained from Freundlich isotherm model was less than 1, indicating that MB was easily adsorbed onto the CM- β -CD-GO.

The effects of temperature on the adsorption of MB onto CM- β -CD-GO were studied at 25 °C, 35 °C, and 45 °C to determine the adsorption nature. The thermodynamic parameters (Gibbs free energy ΔG° , enthalpy ΔH° and entropy ΔS°) were calculated using the following,

$$\Delta G^\circ = \Delta H^\circ - T\Delta S^\circ \quad (8)$$

$$\ln(K_e^\circ) = \frac{-\Delta H^\circ}{R} \frac{1}{T} + \frac{\Delta S^\circ}{R} \quad (9)$$

$$K_e^\circ = \frac{(1000 \cdot K_L \cdot \text{molecular weight of adsorbate} \cdot [\text{adsorbate}]^0)}{\gamma} \quad (10)$$

where R is the gas constant ($8.314 \text{ J mol}^{-1} \text{ K}$), T (K) is absolute temperature, and K_e° is the thermodynamic equilibrium constant that is dimensionless (Lima et al., 2019), γ is the coefficient of activity (dimensionless) and was assumed to be 1 in

this study, $[\text{Adsorbate}]^0$ is the standard concentration of the adsorbate (1 mol L^{-1}), K_L (L mg^{-1}) is a Langmuir adsorption constant.

According to Table 4, the negative ΔG values indicates that the adsorption behavior of CM- β -CD-GO with respect to MB should be a spontaneous reaction. From the positive ΔH values, the adsorption was an endothermic process, and the increase of temperature could promote the adsorption. And it shows that the adsorption process of CM- β -CD-GO to MB possessed chemisorption mechanism. The positive value of ΔS values implies the increment randomness on the solid/solution interface during adsorption. These results indicated that adsorption becomes more favorable at increased temperature.

3.5. Adsorption mechanism

The results of adsorption studies at different pH showed that the removal rate of MB by CM- β -CD-GO increased as the pH and achieved equilibrium after pH 6 was obtained. It indicated that the enhancement of the electronegativity of CM- β -CD-GO was beneficial to adsorbing the positively charged MB, which suggested that electrostatic force drives the adsorption process to a large extent.

As shown in Fig. 3c, the peak of amine (399.90 eV) and N^+ species (401.64 eV) appeared in the high-resolution N1s spectrum of CM- β -CD-GO after MB adsorption. This phenomenon indicated that MB was adsorbed onto the adsorbent surface, and electronic transfer occurred between the amine and N^+ species of MB and the surface of CM- β -CD-GO (Sui et al., 2013). Figs. 3a and b show the high-resolution XPS spectra of C1s and O1s of CM- β -CD-GO before and after MB adsorption. The calculated data are presented in Table S3. The high-resolution C1s spectra indicated changes in the $\text{O}-\text{C}=\text{O}/\text{N}-\text{C}=\text{O}$ groups evidenced by the decreased relative peak intensity compared with those before MB adsorption. In the O1s spectra, the area of $\text{C}=\text{O}/\text{O}-\text{C}=\text{O}$ decreased from 42.61 at% to 30.39 at% after MB adsorption. These changes indicated that MB chemisorption followed the electronic sharing and transfer from these groups to MB and the carboxyl groups was the active sites. Thus, the overall adsorption process was that MB molecule was first

Table 3 Parameters for Langmuir and Freundlich isotherms model.

	Langmuir			Freundlich		
	q_m (mg/g)	K_L (L/mg)	R^2	K_F	n	R^2
25 °C	245.70	2.35	0.9904	141.50	6.53	0.8293
35 °C	260.61	3.40	0.9906	158.11	7.26	0.7707
45 °C	252.44	3.71	0.9771	154.03	7.33	0.7373

Table 4 Thermodynamic parameters for the adsorption of MB on CM- β -CD-GO.

	ΔG (kJ/mol)	ΔH (kJ/mol)	ΔS (J/mol K)
25 °C	-34.01		
35 °C	-35.76	18.10	174.88
45 °C	-37.51		

attracted onto the surface of CM- β -CD-GO by electrostatic action, and further the electron sharing and transfer between the functional groups ($-\text{COOH}$ and $-\text{OH}$) and MB occurred.

The area of C-C/C=C in high-resolution C1s spectra diminished from 37.84 at% to 32.49 at% after MB adsorption. This phenomenon indicates the π - π interaction between the aromatic ring of MB and the skeleton sheet of CM- β -CD-GO (Liu et al., 2014). Many organic compounds containing phenyl groups can enter the cavity of β -CD through the supramolecular interaction between the host and guest (Wang and Zhou, 2007; Jiang et al., 2019). Thus, the inclusion interaction was speculated to also promote the removal of MB by CM- β -CD-GO.

Considering these results, we speculated that the efficient removal of MB by CM- β -CD-GO may be mainly attributed to electrostatic attraction, whereas π - π interaction and host-guest supramolecular interactions also occurred (Fig. 4).

3.6. Desorption and reusability

The excellent recycling performance is expected because it is more conducive to the practical application of adsorbents. Thus, the reusability of CM- β -CD-GO was evaluated by using ethanol as eluent. As shown in Fig. 5, the removal rate

decreased from 98.63% to 82.64%, and the adsorption capacity gradually decreased from 197.26 to 165.25 mg g⁻¹ after five consecutive cycles. This slight decrease in adsorption capacity might be due to the loss of active sites. According to these results, the reusability of CM- β -CD-GO was relatively high.

3.7. Characterization of CM- β -CD-GO

The chemical composition and typical functional group were inspected by XPS analysis. As shown in Fig. 6 and Table S4, the peaks located at 284.6, 531.6, and 398.6 eV represented C1s, O1s, and N1s, respectively. The emerging N1s peak and the increasing of C/O value compared with those of GO proved that β -CD was connected to GO by HDI. The high-resolution C1s and O1s XPS spectra were depicted in Fig. 7, and the calculated data were shown in Table S3. The C1s spectra fitted the four peaks centered at 284.60 (C-C/C=C), 286.56 (C-O), 287.13 (C=O), and 288.16 (O-C=O) eV. For the C1s spectra, the appearance of N-C=O peaks at 288.40 eV indicated that β -CD was successfully anchored onto GO. The $-\text{N}=\text{C}=\text{O}$ of HDI reacted with the hydroxyl groups of β -CD and epoxide and carboxyl groups of GO, respectively. In addition, in the C1s spectra of CM- β -CD-GO, the area of O-C=O/N-C=O was 12.95 at%, which is higher than that of β -CD-GO, indicating the successful introduction of carboxyl groups. Furthermore, in the O1s spectra, the relative C=O/O-C=O oxygen atomic content in CM- β -CD-GO became considerably higher than that in GO. Opposite trends were observed in C-O/C-OH oxygen atomic. These results suggested that the CM- β -CD-GO was successfully prepared.

The FT-IR spectra of the materials were depicted in Fig. 8A. The typical peaks of GO are the stretching vibration

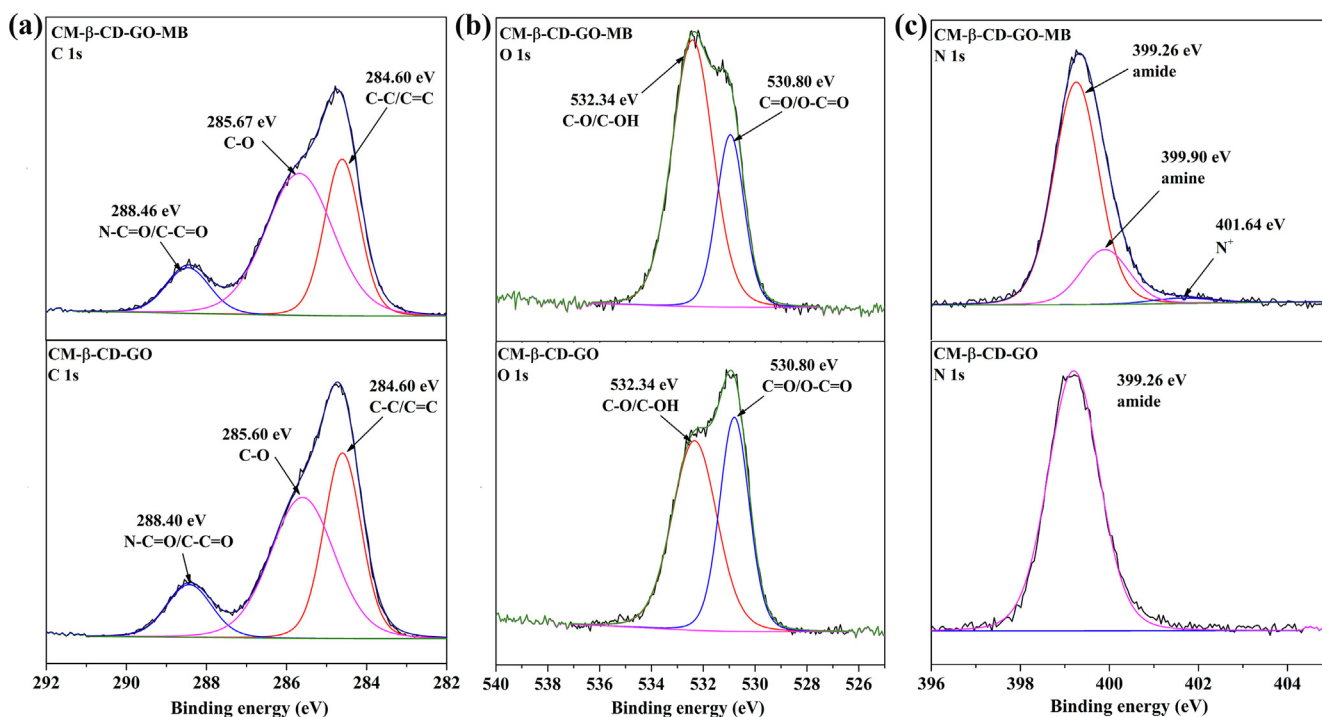


Fig. 3 (a) C1s, (b) O1s and (c) N1s high-resolution XPS spectra of CM- β -CD-GO before and after treatment with MB solution.

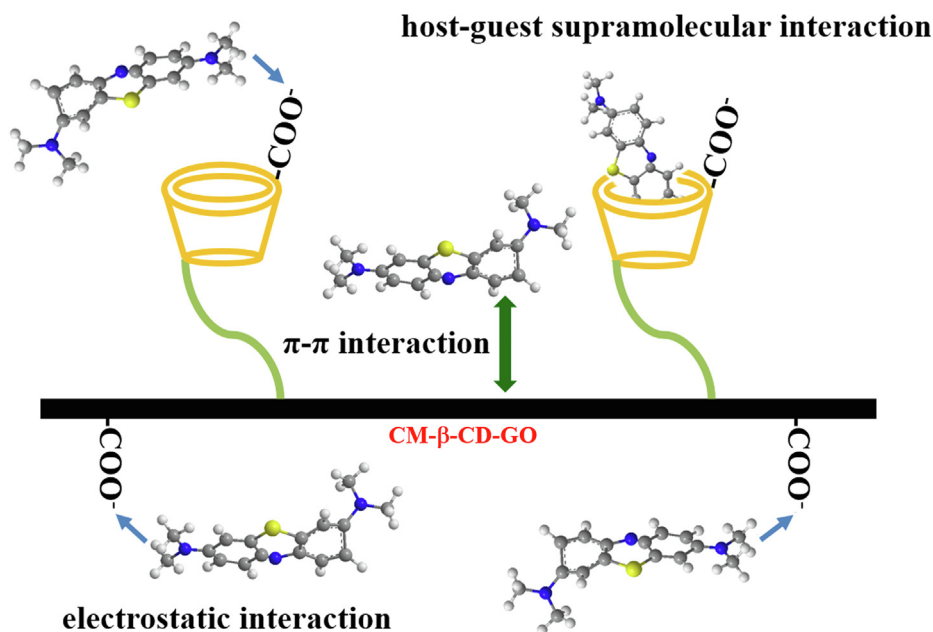


Fig. 4 Proposed adsorption mechanism of MB by CM- β -CD-GO.

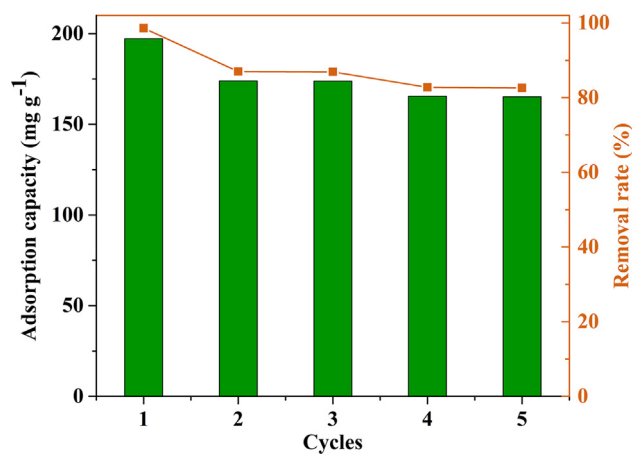


Fig. 5 Reusability of CM- β -CD-GO for MB adsorption.

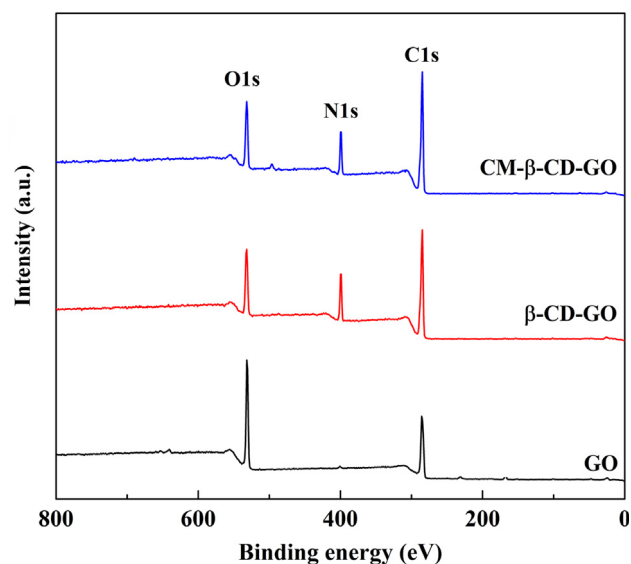


Fig. 6 XPS wide spectra of GO, β -CD-GO and CM- β -CD-GO.

absorption bands of carbonyl ($\sim 1401\text{ cm}^{-1}$), carboxyl ($\sim 1735\text{ cm}^{-1}$) and hydroxyl ($\sim 3407\text{ cm}^{-1}$) groups. The band at 1626 cm^{-1} may belong to the skeletal vibrations of aromatic C=C bonds. The C—O stretching in alkoxy group and epoxy group appearance at 1222 and 1057 cm^{-1} , respectively (Geng et al., 2019). The characteristic peaks of β -CD are R-1, 4-bond skeleton vibration ($\sim 942\text{ cm}^{-1}$), glycoside (C—O—C) ($\sim 1029\text{ cm}^{-1}$) and asymmetric C—H stretching vibration ($\sim 2924\text{ cm}^{-1}$) (Einafshar et al., 2018). The broad absorption band at 3407 cm^{-1} shifted and weakened after modifying GO with β -CD, which might be result from the peaks superposition of O—H and N—H groups. Compared with HDI, the characteristic peaks of —CH₂— appeared at 2933 and 2857 cm^{-1} for the prepared materials, while band at 2253 cm^{-1} (—N=C=O) disappeared. Furthermore, compared with GO, the emerging peaks at 1620 and 1577 cm^{-1} could be attributed to the vibration superposition of —OCONH— and —CONH— groups. The new band at 1255 cm^{-1} belong to

the vibrational peaks of C—O—C in the —OCONH— group. In addition, the peak of glycosidic bond of β -CD appeared in the spectrum of CM- β -CD-GO. The IR spectra of CM- β -CD-GO and β -CD-GO were similar, while the carboxyl peak was masked because of their weakness. Therefore, these results further prove the successful introduction of β -CD onto GO.

TGA curves of materials were shown in Figs. 8B and S3. Weight loss in β -CD-GO occurred in four steps, whereas five weight loss steps were observed in the CM- β -CD-GO curve. The decomposition of water molecules and oxygen-containing functional groups corresponded to the two stages at 30 – $100\text{ }^{\circ}\text{C}$ and 100 – $214\text{ }^{\circ}\text{C}$, respectively. The weight loss of approximately 13.32% at 214 – $291\text{ }^{\circ}\text{C}$ was assigned to the pyrolysis of the attached acetic acid functional groups. The

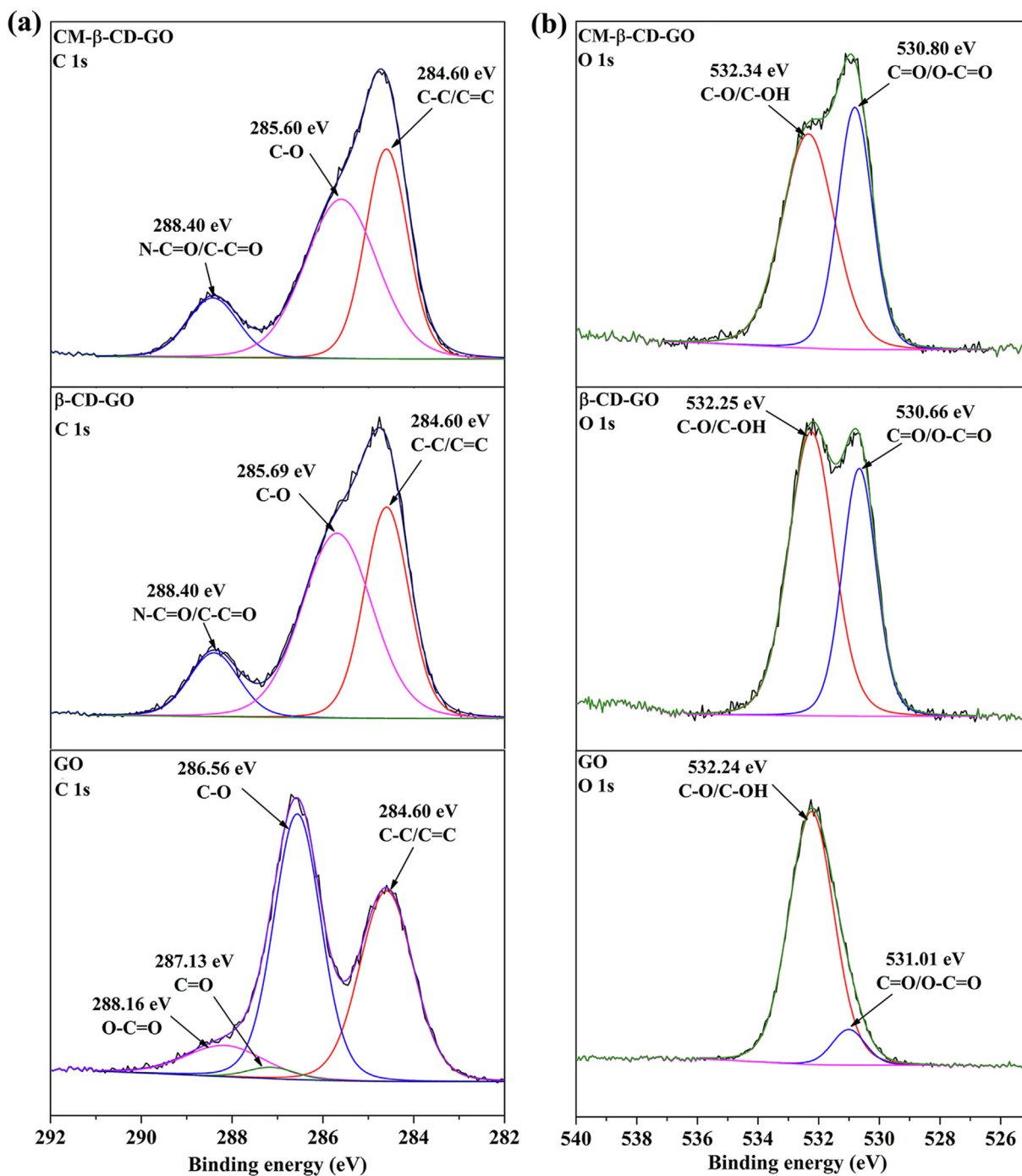


Fig. 7 (a) C1s and (b) O1s high-resolution XPS spectra of GO, β -CD-GO and CM- β -CD-GO.

weight loss regions at 291–389 °C and 389–509 °C for CM- β -CD-GO was due to the decomposition of β -CD and HDI, respectively. These results further indicated the successful grafting of β -CD onto GO and carboxymethylation of β -CD-GO.

As shown in Fig. 8C, the Raman spectrum of GO has two featured peaks at 1356 cm^{-1} (D band) and 1603 cm^{-1} (G band). The extent of disorder could be investigated by the intensity ratio of D (I_D) and G (I_G) bands (Dinda and Saha, 2015). After β -CD modified GO, the I_D/I_G ratio increased from 0.85 to 0.90, demonstrating that β -CD has been intro-

duced into the sp^2 carbon network of GO. Further carboxymethylation of β -CD-GO led to more enhancement of I_D/I_G ratio (0.96), which resulted in the increase of the edges and defects of the adsorbent. This change provided more adsorption sites for MB and made CM- β -CD-GO have excellent adsorption capacity. Fig. 8D shows the XRD pattern, the intense diffraction peak of GO at $2\theta = 9.46^\circ$ with a d spacing of 0.93 nm suggests that GO is rich in oxygen-containing functional groups (Kong et al., 2019). However, after introducing β -CD onto GO, this peak significantly reduced in intensity and shifted to a low angle ($2\theta = 7.67^\circ$) with an interlayer

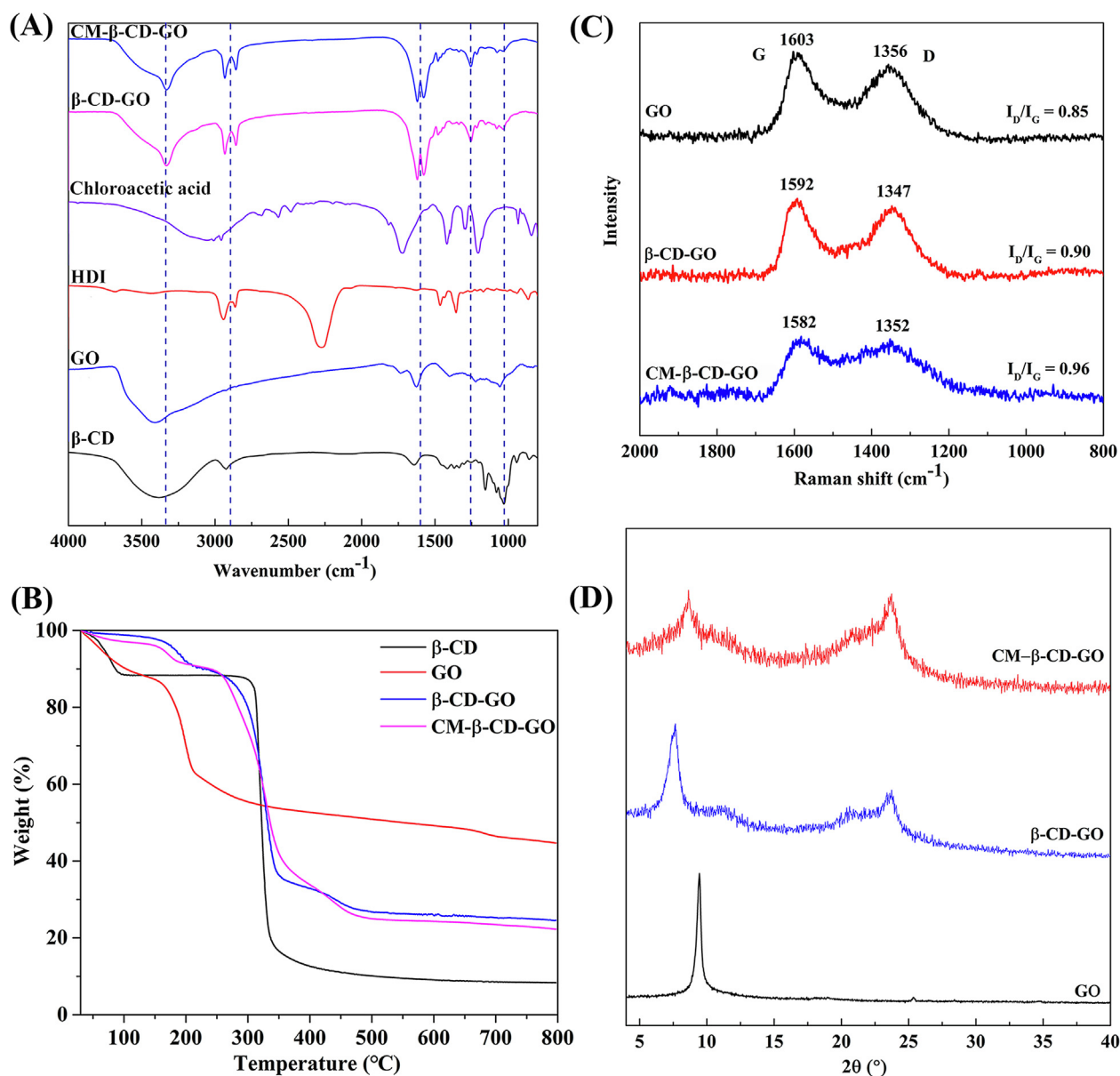


Fig. 8 (A) FT-IR spectra of CM- β -CD-GO, β -CD-GO, chloroacetic acid, HDI, GO, and β -CD; (B) TGA curves of β -CD, GO, β -CD-GO, and CM- β -CD-GO; (C) Raman spectra and (D) XRD pattern of GO, β -CD-GO, and CM- β -CD-GO.

distance of 1.15 nm. The increase in interlayer spacing allowed the adsorbent to capture more adsorbate that lead to an efficient adsorption performance (Mingqian et al., 2018). As for β -CD-GO and CM- β -CD-GO, a broad peak at 23.63° ($d = 0.38$ nm) was observed. This result suggested that several oxygenated groups of GO had been reduced due to the introduction of new functional groups. Moreover, the XRD patterns implied an amorphous state after the interaction of β -CD with GO.

GO and CM- β -CD-GO was characterized by AFM (Eigler et al., 2014; Shearer et al., 2016) and the detail AFM images were shown in Fig. 9. Both GO and CM- β -CD-GO were sheet structures and GO was folded. The height profiles showed that the thickness of single GO was 1.14 nm, the thickness of three layers at the fold was 3.46 nm, and the thickness of CM- β -CD-GO was 1.92 nm. These results indicated that the thickness of

GO increased with the modification of β -CD. The SEM images in Fig. S4 present the microstructure of GO and CM- β -CD-GO. The surface of GO was smooth and the edges was wrinkled (Priya et al., 2018; Ghislandi et al., 2015). CM- β -CD-GO exhibited substantially rougher surface and a thicker layer, and the size was smaller than GO. These microstructural changes were advantageous to MB adsorb onto the surface of adsorbent.

4. Conclusions

In this study, an anionic carboxymethyl functionalized β -CD-modified GO (CM- β -CD-GO) adsorbent for efficiently adsorbing the cationic dye MB from aqueous solutions was fabricated. CM- β -CD-GO showed remarkable adsorption capacities due to the presence of carboxyl functions. The adsorption of MB by CM- β -CD-GO was a rapid process, in which more than 90% of MB could be adsorbed within

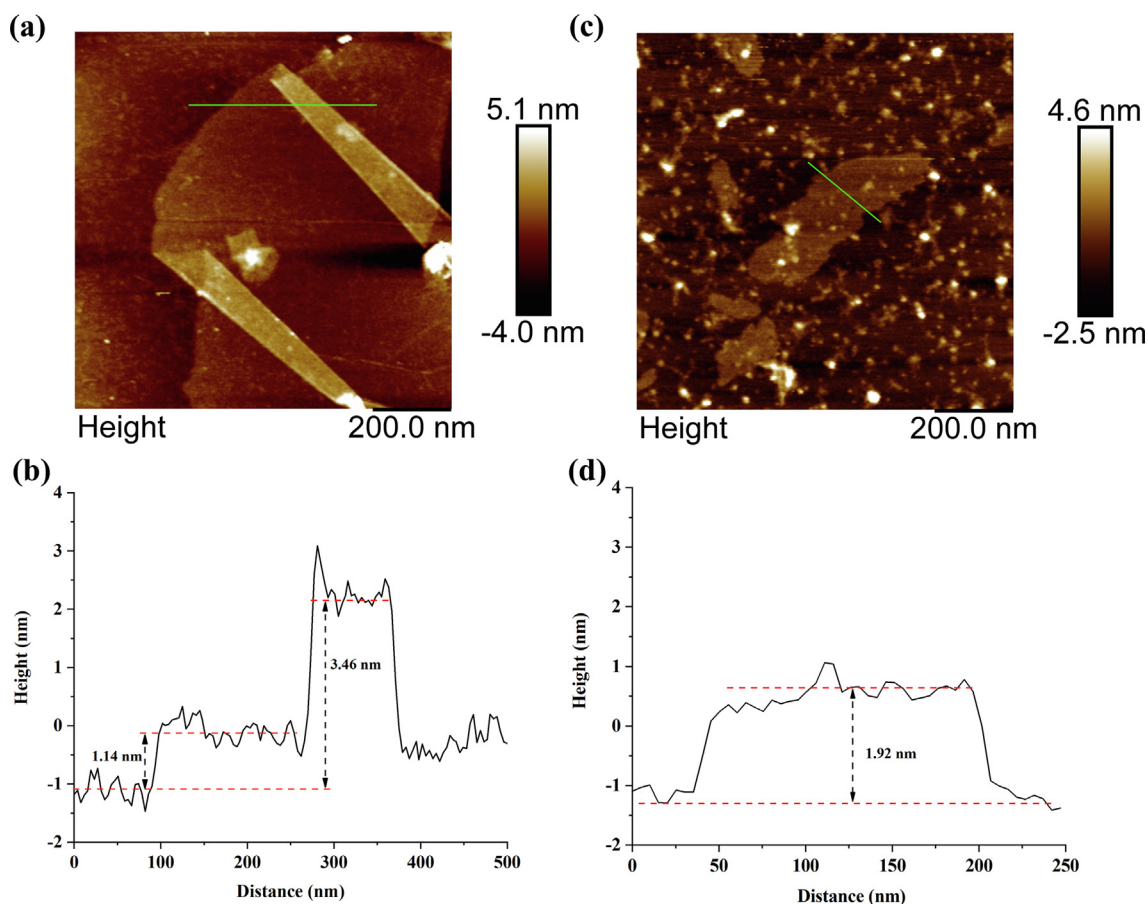


Fig. 9 AFM image of (a) GO and (b) CM-β-CD-GO, the height profile of (a) GO and (b) CM-β-CD-GO.

20 min. CM-β-CD-GO could be applied over a wide range of pH. The mechanism study confirmed that the effective adsorption of CM-β-CD-GO towards MB was driven by the combination of several interactions, among which the electrostatic interaction plays a major role. Kinetics studies demonstrated that the adsorption processes of CM-β-CD-GO with respect to MB could be well described by the pseudo-second-order model, and that the overall process was multi-step-dependent. The cationic dye MB was deposited on the surface of CM-β-CD-GO form a monolayer adsorption, and the adsorption process could occurred spontaneously. Therefore, CM-β-CD-GO is a promising adsorbent in practical application.

Declaration of Competing Interest

The authors declare that there is no conflict of interest regarding the publication of this article.

Acknowledgements

This work was supported by the China Postdoctoral Science Found (Grant no. 2019M653405), the Sichuan Science and Technology Program (Grant no. 2018JY0188), the Fundamental Research Funds for the Central Universities (Grant no. 2018SCU12043).

Appendix A. Supplementary material

Supplementary data to this article can be found online at <https://doi.org/10.1016/j.arabjc.2020.07.008>.

References

- Ali, I., 2012. New generation adsorbents for water treatment. *Chem. Rev.* 112 (10), 5073–5091.
- Alipour, N., Namazi, H., 2018. Removing paraquat and nile blue from aqueous solution using double-oxidized graphene oxide coated by polydopamine nanocomposite. *Int. J. Environ. Sci. Tech.* 16 (7), 3203–3210.
- Badruddoza, A.Z.M., Bhattarai, B., Suri, R.P., 2017. Environmentally friendly β-cyclodextrin–ionic liquid polyurethane-modified magnetic sorbent for the removal of PFOA, PFOS, and Cr (VI) from water. *ACS Sustain. Chem. Eng.* 5 (10), 9223–9232.
- Cerrón-Calle, G.A., Aranda-Aguirre, A.J., Luyo, C., Garcia-Segura, S., Alarcón, H., 2019. Photoelectrocatalytic decolorization of azo dyes with nano-composite oxide layers of ZnO nanorods decorated with Ag nanoparticles. *Chemosphere* 219, 296–304.
- Chen, H., Gao, B., Li, H., 2015. Removal of sulfamethoxazole and ciprofloxacin from aqueous solutions by graphene oxide. *J. Hazard. Mater.* 282, 201–207.
- Chen, J.P., Wu, S., Chong, K.-H., 2003. Surface modification of a granular activated carbon by citric acid for enhancement of copper adsorption. *Carbon* 41 (10), 1979–1986.
- Cheung, W.H., Szeto, Y.S., McKay, G., 2007. Intraparticle diffusion processes during acid dye adsorption onto chitosan. *Bioresour. Technol.* 98 (15), 2897–2904.
- Dinda, D., Saha, S.K., 2015. Sulfuric acid doped poly diaminopyridine/graphene composite to remove high concentration of toxic Cr (VI). *J. Hazard. Mater.* 291, 93–101.
- Einafshar, E., Asl, A.H., Nia, A.H., Mohammadi, M., Malekzadeh, A., Ramezani, M., 2018. New cyclodextrin-based nanocarriers for

- drug delivery and phototherapy using an irinotecan metabolite. *Carbohydr. Polym.* 194, 103–110.
- Eigler, S., Hof, F., Enzelberger-Heim, M., Grimm, S., Müller, P., Hirsch, A., 2014. Statistical Raman microscopy and atomic force microscopy on heterogeneous graphene obtained after reduction of graphene oxide. *J. Phys. Chem. C* 118 (14), 7698–7704.
- Foroutan, R., Mohammadi, R., Ramavandi, B., 2019. Elimination performance of methylene blue, methyl violet, and Nile blue from aqueous media using AC/CoFe₂O₄ as a recyclable magnetic composite. *Environ. Sci. Pollut. Res. Int.* 26 (19), 19523–19539.
- Geissen, V., Mol, H., Klumpp, E., Umlauf, G., Nadal, M., van der Ploeg, M., van de Zee, S.E., Ritsema, C.J., 2015. Emerging pollutants in the environment: a challenge for water resource management. *Int. Soil Water Conserv. Res.* 3 (1), 57–65.
- Geng, J., Yin, Y., Liang, Q., Zhu, Z., Luo, H., 2019. Polyethyleneimine cross-linked graphene oxide for removing hazardous hexavalent chromium: adsorption performance and mechanism. *Chem. Eng. J.* 361, 1497–1510.
- Ghislandi, M., Tkaly, E., Alekseev, A., Koning, C., De With, G., 2015. Electrical conductive behavior of polymer composites prepared with aqueous graphene dispersions. *Appl. Mater. Today* 1 (2), 88–94.
- Jiang, H.L., Lin, J.C., Hai, W., Tan, H.W., Luo, Y.W., Xie, X.L., Cao, Y., He, F.A., 2019. A novel crosslinked β -cyclodextrin-based polymer for removing methylene blue from water with high efficiency. *Colloid. Surf. A* 560, 59–68.
- Karimifard, S., Moghaddam, M.R.A., 2018. Application of response surface methodology in physicochemical removal of dyes from wastewater: a critical review. *Sci. Total Environ.* 640, 772–797.
- Kausar, A., Bhatti, H.N., MacKinnon, G., 2016. Re-use of agricultural wastes for the removal and recovery of Zr(IV) from aqueous solutions. *J. Taiwan Inst. Chem. E* 59, 330–340.
- Khadiji, S.M., Edjlali, L., Akbarzadeh, A., Seyyedi, K., 2019. Enhanced adsorption behavior of amended edta-graphene oxide for methylene blue and heavy metal ions. *Int. J. Environ. Sci. Tech.* 16 (12), 8151–8160.
- Kong, Q., Wei, J., Hu, Y., Wei, C., 2019. Fabrication of terminal amino hyperbranched polymer modified graphene oxide and its prominent adsorption performance towards Cr(VI). *J. Hazard. Mater.* 363, 161–169.
- Kuila, T., Bose, S., Mishra, A.K., Khanra, P., Kim, N.H., Lee, J.H., 2012. Chemical functionalization of graphene and its applications. *Prog. Mater. Sci.* 57 (7), 1061–1105.
- Liu, J., Liu, G., Liu, W., 2014. Preparation of water-soluble β -cyclodextrin/poly(acrylic acid)/graphene oxide nanocomposites as new adsorbents to remove cationic dyes from aqueous solutions. *Chem. Eng. J.* 257, 299–308.
- Lima, E.C., Ahmad, H., Juan, C.M., Ioannis, A., 2019. A critical review of the estimation of the thermodynamic parameters on adsorption equilibria. Wrong use of equilibrium constant in the Van't Hoof equation for calculation of thermodynamic parameters of adsorption. *J. Mol. Liq.* 273, 425–434.
- Mahmoodi, N.M., Abdi, J., Najafi, F., 2013. Gemini polymeric nanoarchitecture as a novel adsorbent: synthesis and dye removal from multicomponent system. *J. Colloid Interf. Sci.* 400, 88–96.
- Mingqian, L., Yan, L., Liu, C., Su, C., Zhou, Q., Zhang, X., Lan, Y., Zheng, Y., Lai, L., Liu, X., Ye, Z., 2018. Non-covalent functionalized graphene oxide (GO) adsorbent with an organic gelator for co-adsorption of dye, endocrine-disruptor, pharmaceutical and metal ion. *Chem. Eng. J.* 349, 791–799.
- Mogha, N.K., Gosain, S., Masram, D.T., 2020. Lanthanum oxide nanoparticles immobilized reduced graphene oxide polymer brush nanohybrid for environmental vitiation of organic dyes. *Arab. J. Chem.* 13 (1), 1367–1376.
- Priya, T., Dhanalakshmi, N., Thennarasu, S., Thinakaran, N., 2018. A novel voltammetric sensor for the simultaneous detection of Cd²⁺ and Pb²⁺ using graphene oxide/ κ -carrageenan/l-cysteine nanocomposite. *Carbohydr. Polym.* 182, 199–206.
- Rathore, E., Biswas, K., 2018. Selective and ppb level removal of Hg (ii) from water: synergistic role of graphene oxide and SnS₂. *J. Mater. Chem. A* 6 (27), 13142–13152.
- Rathour, R.K.S., Bhattacharya, J., Mukherjee, A., 2019. β -Cyclodextrin conjugated graphene oxide: a regenerative adsorbent for cadmium and methylene blue. *J. Mol. Liq.* 282, 606–616.
- Shabaan, O.A., Jahin, H.S., Mohamed, G.G., 2020. Removal of anionic and cationic dyes from wastewater by adsorption using multiwall carbon nanotubes. *Arab. J. Chem.* 13 (3), 4797–4810.
- Soleimani, K., Dadkhah Tehrani, A., Adeli, M., 2018. Preparation of new GO-based slide ring hydrogel through a convenient one-pot approach as methylene blue absorbent. *Carbohydr. Polym.* 187, 94–101.
- Sui, Z.Y., Cui, Y., Zhu, J.H., Han, B.H., 2013. Preparation of three-dimensional graphene oxide-polyethylenimine porous materials as dye and gas adsorbents. *ACS Appl. Mater. Interfaces* 5 (18), 9172–9179.
- Shearer, C.J., Slattery, A.D., Stapleton, A.J., Shapter, J.G., Gibson, C. T., 2016. Accurate thickness measurement of graphene. *Nanotechnology* 27, (12) 125704.
- Tang, P., Sun, Q., Zhao, L., Tang, Y., Liu, Y., Pu, H., Gan, N., Liu, Y., Li, H., 2019a. A simple and green method to construct cyclodextrin polymer for the effective and simultaneous estrogen pollutant and metal removal. *Chem. Eng. J.* 366, 598–607.
- Tang, Y., Li, M., Mu, C., Zhou, J., Shi, B., 2019b. Ultrafast and efficient removal of anionic dyes from wastewater by polyethyleneimine-modified silica nanoparticles. *Chemosphere* 229, 570–579.
- Uddin, M.T., Islam, M.A., Mahmud, S., Rukanuzzaman, M., 2009. Adsorptive removal of methylene blue by tea waste. *J. Hazard. Mater.* 164 (1), 53–60.
- Wang, Y., Zhou, A., 2007. Spectroscopic studies on the binding of methylene blue with DNA by means of cyclodextrin supramolecular systems. *J. Photoch. Photobio. A* 190 (1), 121–127.
- Weber, W.J., Morris, J.C., 1963. Kinetics of adsorption on carbon from solution. *J. Sanit. Engin. Div.* 89 (2), 31–60.
- Yao, G., Li, S., Xu, J., Liu, H., 2019. Dual-responsive graphene oxide/poly(nipam-co-aa) hydrogel as an adsorbent for rhodamine b and imidacloprid. *J. Chem. Eng. Data* 64 (9), 4054–4065.
- Zhang, C., Li, Y., Li, Y., Zhang, W., Wang, X., He, X., Yu, M., 2019. Synthesis and Zn (II) modification of hierarchical porous carbon materials from petroleum pitch for effective adsorption of organic dyes. *Chemosphere* 216, 379–386.
- Zhu, Y., Yi, C., Zhu, J., Han, B., 2013. Preparation of three-dimensional graphene oxide-polyethylenimine porous materials as dye and gas adsorbents. *ACS Appl. Mater. Interfaces* 5, 9172–9179.